Temperature distributions and their evolution in non-planar energy beam microprocessing: A fast algorithm

N. Arnold[a)]
Angewandte Physik, Johannes-Kepler-Universität, Linz, A-4040, Linz, Austria

(Received 7 August 1995; accepted for publication 17 April 1996)

We present a fast algorithm for calculations of the temperature distributions induced by the energy beam in the three-dimensional deposits of arbitrary shape. It combines analytical approximations, numerical fast Fourier transform, and the multigrid technique. The accuracy of the method is demonstrated with problems that can be solved analytically. The behavior of the center temperature in laser-deposited spots and stripes of different shapes and sizes is studied. The results can explain explosive growth in laser-induced deposition and instabilities in laser direct writing, and provide a tool for a quantitative analysis of energy beam microprocessing. © *1996 American Institute of Physics.* [S0021-8979(96)08614-8]

I. INTRODUCTION

Microprocessing[1–3] by means of laser and electron beams becomes an increasingly versatile tool in microelectronics, micromachining, and micromechanics. The knowledge of the beam-induced temperature distribution is a prerequisite for the understanding of kinetics of the underlying pyrolytic processes. Experimental measurements of the temperature are difficult mainly because of the small area of the processed zone, changes in its geometry, and the necessity to perform it without direct contact (see e.g., review[4] and references therein). For these reasons, calculated temperature distributions are often quite useful. Here, one can distinguish between the two cases.

In some processes, the change in the geometry of the specimen is easily incorporated in computational algorithm. The examples are the doping of plane surfaces or the deposition of *homogeneous* films. In such cases analytical and numerical solutions[5–9] can be applied, some of them include multilayer structures,[10] different shapes of the energy beam,[11] temperature dependent material parameters, melting, etc.

In other applications, the geometry within the processed zone changes dramatically. Examples are drilling, cutting, etching and deposition of patterns with high aspect ratios, e.g., in three-dimensional (3D) fabrication of devices in microelectronics or micromechanics.[12,13]

Temperature calculations for such systems were performed numerically,[14,17] often by assuming a fixed geometry. This does not allow to model deposition or etching. In Refs. 18,19 the temporal behavior of the deposition process *was* simulated and some non-trivial shapes like valleys in the center of deposits (due to decrease of the deposition rate with temperature) were reproduced. This procedure, however, requires the use of supercomputers. In Ref. 20 we proposed a *one-dimensional* (1D) analytical model for laser direct writing, which permits also to describe oscillations and discontinuous deposition.[21,22] This approach proved to be suitable for a *qualitative* explanation of experimental results, but it does not always provide *quantitative* agreements. For a quantitative description a *two-dimensional* (2D) approach[23] for *thermally thin* deposits is more promising. However, in many processing situations the assumption of thermally thin patterns is violated. Moreover, for some effects temperature variations *within deposits* are crucial. Besides, the computational algorithm used in Ref. 23, although by far superior to the direct finite differences or finite element solution of a 3D problem, was still rather slow for extensive simulations and an analysis of experimental results.

In this article we generalize the approach of Ref. 23 to include thermally thick deposits, derive the equations which can be used to calculate the temperature distribution with arbitrary accuracy, and study in detail the approximation which suffices for many practical purposes. The numerical method combines fast Fourier transform (FFT) for calculating 2D convolutions, and the multigrid method of solution for the 2D elliptical equation with non-constant coefficients.

II. MODEL

We consider the situation schematically shown in Fig. 1. The deposit with thermal conductivity $K_D(T)$ occupies the region $0<z<h(x,y)$ on a semi-infinite substrate with thermal conductivity $K_S(T)$. The incident energy beam can be absorbed within both the deposit and the substrate. We assume that the temperature distribution $T(x,y,z)$ can be determined from the stationary heat equation. This is a good approximation in *micro*processing where typical heat velocities are much greater than characteristic scanning velocities of the energy beam or the growth or etch rate.

The heat conductivities can depend on temperature in an *arbitrary* way. This is handled via the Kirchhoff transforms for substrate and deposit. Kirchhoff transform with respect to $K(T)$ is given by:

$$\theta(T)=\frac{1}{K(T_0)}\int_{T_0}^{T}K(T')dT'.$$

It makes *stationary* heat conduction equation *linear*[5,7] with respect to *linearized temperature* θ. Here T_0 is the ambient temperature. *Inverse* Kirchhoff transform yields $T(\theta)$ dependence. With these assumptions the thermal problem can be written as:

a)Electronic mail: nikita.arnold@jk.uni-linz.ac.at

 0021-8979/96/80(3)/1291/8/$10.00

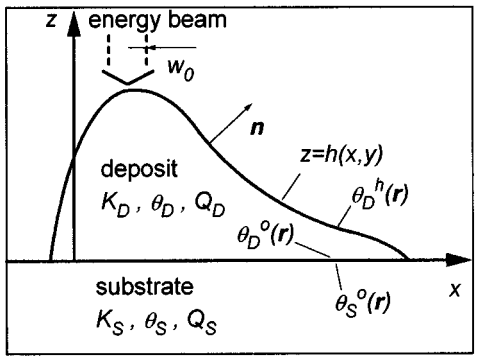

FIG. 1. Schematic picture of a 2D model for the temperature calculations. y-axis is perpendicular to the plane of the figure. The surface of the deposit is at $z=h(x,y)$. $\mathbf{n}$ is the normal to this surface and $\mathbf{r}$ is 2D radius vector in (x,y)-plane.

$$K_D\left(\frac{\partial^2\theta_D}{\partial z^2}+\nabla^2\theta_D\right)+Q_D=0, \tag{2.1a}$$

$$K_S\nabla_3^2\theta_S+Q_S=0, \tag{2.1b}$$

$$\left.\frac{\partial\theta_D}{\partial\mathbf{n}}\right|_{z=h(x,y)}=\mathbf{n}\nabla_3\theta_D|_{z=h(x,y)}=[1+(\nabla h)^2]^{-1/2}\times\left(\frac{\partial\theta_D}{\partial z}-\nabla h\cdot\nabla\theta_D\right)\Bigg|_{z=h(x,y)}=0, \tag{2.2a}$$

$$\theta_S|_{z\to-\infty}=\theta_S|_{|x|,|y|\to\infty}=0, \tag{2.2b}$$

$$K_D\left.\frac{\partial\theta_D}{\partial z}\right|_{z=0}=K_S\left.\frac{\partial\theta_S}{\partial z}\right|_{z=0}, \tag{2.2c}$$

$$T(\theta_D|_{z=0})=T(\theta_S|_{z=0}). \tag{2.2d}$$

Here, θ_D and θ_S refer to the deposit and substrate respectively and $K_S\equiv K_S(T_0), K_D\equiv K_D(T_0)$ are constant. ∇_3^2 is 3D Laplacian and ∇^2 and ∇ are 2D Laplacian and 2D nabla operator. The derivative with respect to z was extracted from ∇_3^2 in Eq. (2.1a) in order to perform averaging later in Sec. III. Q_D and Q_S are (volume) source terms (θ-dependent if the optical properties of the materials depend on temperature). $\mathbf{n}$ is the unit (outward) normal to the surface of the deposit (Fig. 1):

$$\mathbf{n}=(n_x,n_y,n_z)=[1+(\nabla h)^2]^{-1/2}\left(-\frac{\partial h}{\partial x},-\frac{\partial h}{\partial y},1\right). \tag{2.3}$$

In Eq. (2.2a) we neglect heat losses from the upper surface. Equation (2.2c) reflects the continuity of the heat flux across the interface, and Eq. (2.2d) the continuity of the temperature.

It is attractive to reduce 3D system in Eqs. (2.1)–(2.2) to a set of 2D equations which allow to calculate the (linearized) temperature at the *surface* of the deposit $\theta_D^h(x,y)\equiv\theta_D(x,y,z=h(x,y))$. One way is to write Green's formula[24] for the deposit and substrate. This approach gives a system of integro-differential equations for the temperatures and the normal derivatives *at all the interfaces.* This system is 2D and it is *exact*, but its integrals do not have the form of convolutions, as the integrals presented in Sec. III. This does not allow to use FFT methods for their calculations, which dramatically slows down the numerical algorithm.

Below we adopt different approach, based on averaging procedure.

III. ANALYTICAL CONSIDERATION

Solving Eq. (2.1b) within the *substrate* using Green's function technique[25] we have for $z=0$:

$$\theta_S^0\equiv\theta_S(x,y,0)=\frac{1}{2\pi}\left\{\theta_S'*\frac{1}{r}\right\}+\frac{1}{2\pi}\int_{-\infty}^{0}\int_{-\infty}^{\infty}\int_{-\infty}^{\infty}\frac{Q_S(\mathbf{r}',z')dz'd^2\mathbf{r}'}{(|\mathbf{r}-\mathbf{r}'|^2+z'^2)^{1/2}}. \tag{3.1}$$

Here, θ_S^0 denotes the linearized temperature of the substrate at $z=0$, θ_S' the derivative with respect to z at $z=0$, $\{*\}$ denotes the 2D convolution integral, $\mathbf{r}$ and $\mathbf{r}'$ are the radius vectors in (x,y) and (x',y') planes, and r,r' are their lengths. The last integral in Eq. (3.1) is often either absent (transparent substrate or everything is absorbed within the deposit), or the integration over z' can be approximated and/or performed analytically, so that the remaining integral has the form of 2D convolution. θ_S' in Eq. (3.1) should be derived from the heat conduction equation for the deposit.

Now we perform certain averaging. We multiply Eq. (2.1a) by an arbitrary function $f(z)$ and integrate the result over dz from $z=0$ to $z=h(x,y)\equiv h(\mathbf{r})$, which we henceforth denote as h. We integrate the first term by parts and use the boundary conditions Eqs. (2.2a) and (2.2c) to eliminate z-derivatives at $z=0$, h:

$$K_Df(h)\nabla h\cdot\nabla\theta_D|_{z=h}-K_Sf(0)\theta_S'+K_D\left[-\int_0^h f'\theta_D'dz+\int_0^h f\nabla^2\theta_D dz\right]+\int_0^h fQ_D dz=0. \tag{3.2}$$

Here, f', θ_D' denote z-derivatives. The first term in Eq. (3.2) and the second term in square brackets can be combined, and we can substitute:

$$\theta_D(x,y,z)=\theta_D^0(x,y)+\theta_D^1(x,y,z),\quad \theta_D^1(x,y,0)\equiv 0. \tag{3.3}$$

Here θ_D^0 is the temperature of the deposit at the interface $z=0$. This yields:

$$K_Sf(0)\theta_S'=\int_0^h fQ_Ddz+K_D\nabla\left[\left(\int_0^h fdz\right)\cdot\nabla\theta_D^0\right]+K_D\left[\nabla\left(\int_0^h f\nabla\theta_D^1dz\right)-\int_0^h f'\theta_D^{1\prime}dz\right]. \tag{3.4}$$

Equation (3.4) is *exact* and valid for arbitrary function $f(z)$. It is possible to expand θ_D in Eq. (3.3) in a series of z-dependent functions $f_i(z)$, substitute it into Eq. (3.4) and

perform averaging over z with each of these functions f_i used as a weight function f in Eq. (3.4). This results in an (infinite) set of equations for the (x,y) dependent coefficients in this expansion, which approximate θ_D with arbitrary precision.

We will use f_0, f_1 which arise from the *first two terms* of the Taylor expansion of θ_D in z-coordinate. The resulting pair of equations has a clear physical meaning and, as it is shown in Sec. IV, it provides a good approximation to the whole problem for a wide range of parameters. Namely, we assume:

$$\theta_D(x,y,z) \equiv \theta_D^0(x,y) + \theta_D^1(x,y,z) = f_0(z)\,\theta_D^0(x,y) + f_1(z)\,\theta_1(x,y), \tag{3.5}$$

$$f_0(z) \equiv 1, \tag{3.6a}$$

$$f_1(z) \equiv z. \tag{3.6b}$$

Equation (3.4) written for $f=f_0$ and $f=f_1$ gives two Galerkin (or variational) equations[26,27] for the trial solution (3.5):

$$K_S\theta_S' = \int_0^h Q_D dz + K_D\nabla(h\nabla\theta_D^0) + K_D\nabla\left(\frac{h^2}{2}\nabla\theta_1\right), \tag{3.7a}$$

$$K_D^{-1}\int_0^h zQ_D dz + \nabla\left(\frac{h^2}{2}\nabla\theta_D^0\right) + \nabla\left(\frac{h^3}{3}\nabla\theta_1\right) = h\theta_1. \tag{3.7b}$$

The physical meaning of these equations can be illustrated as follows. With $h\to 0$ we can neglect the last term in Eq. (3.7a). The resulting equation is the energy balance within the thermally thin deposit. The second term in the right side represents the lateral ''spreading'' of the surface temperature due to the presence of the deposit.[23] The last term in Eq. (3.7a) gives further correction to the approximation of a thin deposit.

In order to elucidate the meaning of Eq. (3.7b), let us again consider $h\to 0$, and assume that Q_D is absorbed on the upper surface of the deposit $z=h$. Then, Eq. (3.7b) degenerates into $K_D\theta_1 = I_A$, where I_A is the total absorbed intensity. But from Eqs. (3.5) and (3.6), θ_1 is just z-derivative of the temperature, and thus, Eq. (3.7b) is the condition of flux conservation. Note, that the right side of Eq. (3.7b) is the temperature difference within the deposit $\theta_D^h - \theta_D^0$.

In the general case, Eqs. (3.7) are coupled. θ_1 should be found from Eq. (3.7b) and substituted into Eq. (3.7a) which yields θ_S'. Then, θ_S' should be inserted into Eq. (3.1). θ_S^0 in Eq. (3.1) should be considered as the function of θ_D^0:

$$\theta_S^0 \equiv \theta_S^0(\theta_D^0) = T_S^{-1}[T_D(\theta_D^0)]. \tag{3.8}$$

Here, $T_D(\theta_D^0)$ is given by the *inverse* Kirchhoff transform with respect to *deposit*, and T_S^{-1} is *direct* Kirchhoff transform with respect to the *substrate*. Equation (3.8) is the condition (2.2d) of temperature continuity, rewritten in terms of θ_D and θ_S.[23] Thus, Eq. (3.1) becomes nonlinear integrodifferential equation for the determination of θ_D^0. Once θ_D^0 has been found, θ_1 and θ_D^h can be determined from Eqs. (3.7b) and 3.5) with $z=h$ (see Eq. (4.2)).

IV. NUMERICAL PROCEDURE

Let us enumerate the advantages of the system of Eqs. (3.1), (3.7), (3.8).

(i) It is 2D instead of 3D in the initial problem.

(ii) Integrations in Eqs. (3.1) and (3.7) are confined to the regions where Q or h are non-zero, although the *temperature* at the boundaries of this region is still much higher than T_0. Thus, no boundary conditions for θ at *infinity* should be considered in the *numerical* algorithm. This leads to a big decrease in the size of the discretized region.

(iii) No boundary conditions of the type of Eqs. (2.2c) or (2.2a) on the non-planar surface should be considered. This is particularly advantageous for problems where h changes with time.

(iv) The form of Eqs. (3.7b) and (3.1) allows to use such methods as multigrid and FFT,[28] which speed up the calculation by about two *orders* of magnitude.

(v) Even with *arbitrary* dependences $K_D(T), K_S(T)$ the algorithm remains essentially linear.

The sequence of steps in the numerical solution is the following. Equation (3.1) is solved iteratively with respect to θ_D^0. Symbolically it can be written as:

$$\theta_{D,i+1}^0 = \theta_{D,i}^0 + c\left[\frac{1}{2\pi}\left\{\theta_S'(\theta_{D,i}^0, \theta_1(\theta_{D,i}^0)) * \frac{1}{r}\right\} + I_S[\theta_S^0(\theta_{D,i}^0)] - \theta_S^0(\theta_{D,i}^0)\right]. \tag{4.1}$$

Here, index i denotes the number of iteration, and different θ are functions (arrays in numerical realization). The expression in outer square brackets is Eq. (3.1). I_S denotes the last integral in Eq. (3.1). c is constant coefficient introduced to ensure convergence. The function $\theta_S'(\theta_D^0, \theta_1)$ is defined explicitly by Eq. (3.7a). The function $\theta_1(\theta_D^0)$ is *implicitly* defined by Eq. (3.7b). In order to find θ_1 from θ_D^0, the elliptic problem of Eq. (3.7b) is solved by multigrid technique. The function $\theta_S^0(\theta_D^0)$ is given by Eq. (3.8). The convolutions are calculated by FFT method. Obviously, some of the functions in Eq. (4.1) depend on the array of height h via Eq. (3.7). After θ_D^0 and θ_1 have been found, the temperature at the surface of the deposit can be written by inverse Kirchhoff transform of θ_D^h which is given by Eq. (3.5) with $z=h$

$$T|_{z=h} = T_D(\theta_D^h) = T_D(\theta_D^0 + h\theta_1). \tag{4.2}$$

This formula should also be used in Eq. (4.1) during the calculation if, for example, the absorptivity of the deposit depends on surface temperature.

There exist some subtleties in the numerical procedure which we briefly outline below.

The convolution integral in Eq. (4.1) has a singularity at $\mathbf{r}=0$ which makes it sensitive to the choice of the mesh. One mesh point was placed at $\mathbf{r}=0$ with the r^{-1} value given by the integration over the rectangle $-0.5\times dx < x < 0.5\times dx$, $-0.5\times dy < y < 0.5\times dy$, where dx and dy are the spatial steps:

$$r^{-1}_{discret.}(\mathbf{r}=0)=2\left(dy^{-1}\ln\left\{\frac{dy}{dx}+\left[1+\left(\frac{dy}{dx}\right)^2\right]^{1/2}\right\}\right.$$
$$\left.+dx^{-1}\ln\left[\frac{dx}{dy}+1+\left(\frac{dx}{dy}\right)^2\right]^{1/2}\right). \quad (4.3)$$

FFT works only on a uniform mesh. Thus dx,dy = const., which can be considered as a disadvantage of our method. Nevertheless, the decrease in computational time provided by the FFT an multigrid routines pays off this limitation. In Eq. (4.1) two functions are convoluted $-r^{-1}$, which has infinite support, and θ'_S, which, as it can be seen from Eq. (3.7), is equal to zero outside the regions where intensity and height have non-zero values. This is exactly the region where we want to calculate the temperature distribution. In order not to spoil the result of convolution by edge effects, one has to consider the region twice as big in x,y coordinates. The function θ'_S should be padded with zeros in this region, and stored in wrap around order,[28] whereas r^{-1} should be calculated in a normal way.

The FFT works efficiently when the number of mesh points in one coordinate is $N=2^n$. The multigrid method[28] works best if $N=2^m+1$. To satisfy both requirements, the grid was extended one point for each coordinate when Eq. (3.7b) was solved to determine θ_1.

The coefficient c in Eq. (4.1) ensures convergence of the iterations. If c is not small enough, instability arises, which is analogous to that of the explicit schemes in parabolic time-dependent equations: The most ''dangerous'' region for the discretization (4.1) of Eqs. (3.1) and (3.7) is the area $dS\sim dx\ dy$ near $\mathbf{r}=0$, where $r^{-1}\sim\max(dx^{-1},dy^{-1})$, and h is a slowly varying function. The discretization of the second derivatives in Eq. (3.7a) and substitution of θ'_S into Eq. (4.1) can be schematically written as:

$$\frac{\theta^0_{D,i+1}-\theta^0_{D,i}}{c}\approx\frac{1}{2\pi}\frac{K_D}{K_S}\frac{hdS}{\min(dx,dy)}\nabla^2\theta^0_{D,i}+\dots . \quad (4.4)$$

Applying Courant stability criterion[28] to Eq. (4.4), we get the restriction on c:

$$c\leqslant\min\left(1,c_1\frac{K_S}{K_D}\frac{\min(dx,dy)}{h_{\max}}\right). \quad (4.5)$$

Coefficient $c_1\approx1$ arises from the approximations made, omitted terms in Eq. (4.4), and should be determined numerically. $h_{\max}$ is the maximum value of height. The value of $c=1$, provides the fastest possible convergence for $h=0$, although the scheme is stable up to $c=2$. With small c the convergence is slow, therefore c should be taken as big as possible, using Eq. (4.5) as an estimation.

The program was written in FORTRAN. With typical values $K_S/K_D\approx1$, $dx/h_{\max}\approx0.1$, the calculations up to 10^{-5} accuracy on 64×64 grid required from 1 s to about 1 min on the Pentium 90 CPU.

V. VALIDATION OF THE APPROXIMATIONS AND ALGORITHM

The program was tested on the problem with the analytical solution—the case of *uniform* height h and fixed ratio of heat conductivities $K^*=K_D(T)/K_S(T)$ which leads to $\theta^0_S\equiv\theta^0_D$ in Eq. (3.8). Here we present the solutions for the center (linearized) temperature at the upper surface of the deposit $\theta^h_D(0)\equiv\theta^h_D(\mathbf{r}=0)$. We assume Gaussian beam $I(\mathbf{r})=I_0\exp(-r^2/w_0^2)$ with spot size w_0, and surface absorptivity A. More general solutions are given in Ref. 8. For the *surface* absorption in the *deposit*

$$\frac{\theta^h_D(0)K_S}{AI_0w_0}=\frac{1}{2}\int_0^\infty e^{-k^2/4}\times\frac{ch(kh/w_0)+K^{*-1}sh(kh/w_0)}{ch(kh/w_0)+K^*sh(kh/w_0)}\,dk \quad (5.1a)$$

for *surface* absorption in the *substrate*:

$$\frac{\theta^0_D(0)K_S}{AI_0w_0}=\frac{1}{2}\int_0^\infty e^{-k^2/4}\frac{dk}{ch(kh/w_0)+K^*sh(kh/w_0)} \quad (5.1b)$$

and for the Bouger absorption with the absorption coefficient a within the deposit only:

$$\frac{\theta^h_D(0)K_S}{AI_0w_0}=\frac{1}{2}\int_0^\infty e^{-k^2/4}\frac{\alpha^2}{\alpha^2-k^2}\left[\frac{ch(kh/w_0)+K^{*-1}sh(kh/w_0)}{ch(kh/w_0)+K^*sh(kh/w_0)}\left\{1-\left(\frac{k}{\alpha}sh(kh/w_0)+ch(kh/w_0)\right)e^{-\alpha h}\right\}\right.$$
$$\left.+K^{*-1}\left(sh(kh/w_0)+\frac{k}{\alpha}\right)e^{-\alpha h}-K^{*-1}\frac{k}{\alpha}\right]dk. \quad (5.1c)$$

The source terms in Eq. (3.7) for these cases are given by

$$\int_0^h Q_D dz=\begin{bmatrix}AI(\mathbf{r})\\ AI(\mathbf{r})\\ AI(\mathbf{r})(1-e^{-\alpha h})\end{bmatrix}, \quad \int_0^h zQ_D dz=\begin{bmatrix}AI(\mathbf{r})h & (5.2a)\\ 0 & (5.2b)\\ AI(\mathbf{r})h[1-(\alpha h)^{-1}(1+e^{-\alpha h})]. & (5.2c)\end{bmatrix}$$

TABLE I. The comparison between the analytical (Eq. (5.1)) and numerical (Eqs. (3.1) and (3.7)) solutions for $h=$const. The numbers show the normalized center temperature rise at the surface of the deposit $\theta_D^h(0)K_S/I_0Aw_0$ for different values of $K^*\equiv K_D/K_S$ and h/w_0.

h/w_0	0.01		0.1		0.3		1	
K^* absorption	analyt.	numer.	analyt.	numer.	analyt.	numer.	analyt.	numer.
0.1 surface $z=0$	0.9850	0.9758	1.8469	1.8383	3.4600	3.4440	6.2214	5.8026
surface $z=h$	0.8851	0.8759	0.8681	0.8592	0.7973	0.7877	0.5291	0.4827
Bouger, $\alpha h=3$	0.9093	0.8972	1.4907	1.4529	2.5272	2.4753	3.7674	3.9170
1 surface $z=0$	0.8862	0.8772	0.8862	0.8789	0.8862	0.8762	0.8862	0.8358
surface $z=h$	0.8763	0.8673	0.7945	0.7870	0.6510	0.6415	0.3789	0.3499
Bouger, $\alpha h=3$	0.8394	0.8305	0.8165	0.8076	0.7700	0.7621	0.6350	0.6363
10 surface $z=0$	0.8016	0.7943	0.4871	0.4852	0.3019	0.2989	0.1693	0.1575
surface $z=h$	0.8007	0.7934	0.4801	0.4781	0.2845	0.2815	0.1269	0.1158
Bouger, $\alpha h=3$	0.7615	0.7545	0.4605	0.4589	0.2804	0.2788	0.1412	0.1371

In Table I we present the values of $\theta_D^h(0)K_S/AI_0w_0$ for different K^* and h/w_0 for three types of absorption given by Eq. (5.1). For each h/w_0 ratio the left column shows the analytical solutions (5.1), and the right one the numerical result. Three rows for each value of K^* refer to the cases a, b, c in Eqs. (5.1) and (5.2). With thermally thin deposits and/or moderate ratios h/w_0 the results are indistinguishable.

Figure 2 shows the analytical solution and the approximate values of $\theta_D^0(r)$ and $\theta_D^h(r)$ for $h/w_0=1$, $K^*=1$. There is a good agreement for all r. Similar behavior is observed for other values of $h/w_0, K^*$, with the accuracy illustrated in Table I.

One more note is appropriate here. The assumption (3.5) is better fulfilled for the spatially *confined* deposits than $h=$const where the heat may spread wider within the deposit. Correspondingly, the accuracy of the algorithm is better for the confined deposits.

VI. EXAMPLE: TEMPERATURE DISTRIBUTIONS IN THE SPOTS AND STRIPES

As a nontrivial application of the algorithm we consider deposited spots and stripes irradiated by the Gaussian beam $I(\mathbf{r})=I_0\exp(-r^2/w_0^2)$. To emphasize the essential features of temperature distributions, we assume *surface* absorption in the deposit with $A=$const, and $\theta_S^0\equiv\theta_D^0$ in Eq. (3.8) as in Sec. V. First, we consider the spots of the generalized parabolic shape (see also inset in Fig. 5):

$$h(r)=\begin{cases} h_0(1-(r/R)^{2m}), & r<R \\ 0, & r>R \end{cases}. \tag{6.1}$$

$m=1/2$ corresponds to a cone, $m=1$ to a paraboloid, $m\gg 1$ to a nearly cylindrical spot.

In Fig. 3 we show the influence of the shape of the deposit determined by the parameter m on $\theta_D^h(r)$ and $\theta_D^0(r)$. The influence is weak with $K^*=10$, and increases for $K^*=1$. The dependence of *temperature* T on shape may be more pronounced when linearized temperature θ_D^h is recalculated into T via inverse Kirchhoff transform $T_D(\theta_D)$, if $T_D(\theta_D)$ is a strongly increasing function. This is the case for semiconductors, which heat conductivity $K(T)$ strongly *decreases* with T.[29]

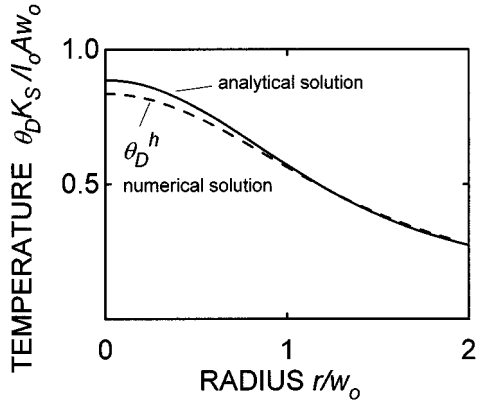

FIG. 2. Normalized distribution $\theta_D(r)$ for constant height $h(r)=1$, $K^*=1$ and surface absorption in the deposit. Solid line—analytical solution (5.1a). Dashed line—numerical result for $\theta_D^h(r)$. w_0 is the radius of (Gaussian) beam.

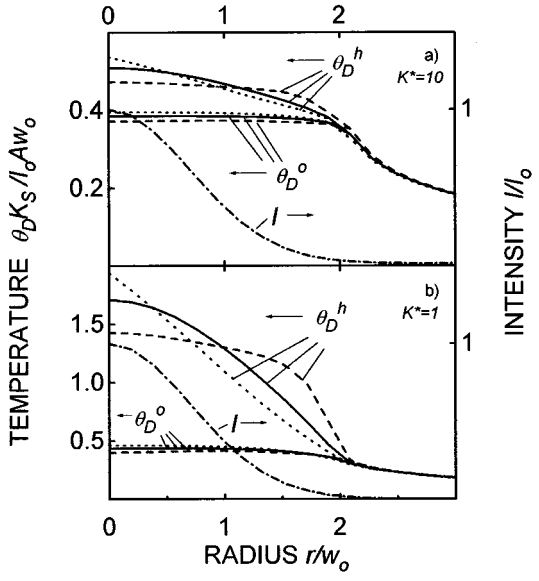

FIG. 3. The influence of the shape of the spot on the temperature distributions $\theta_D^h(r), \theta_D^0(r)$. Solid lines—paraboloid spot ($m=1$), dashed lines—nearly cylindrical spot ($m=4$), dotted lines—cone ($m=0.5$). Normalized intensity is plotted by dash-dotted line. For all curves $R/w_0=2$, $h_0/w_0=3$ and surface absorption within the deposit (Eq. (5.2a)) have been employed.

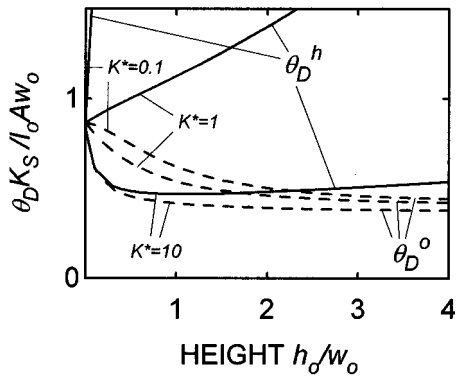

FIG. 4. The dependence of the (normalized) *center* temperature rise at the surface of the deposit $\theta_D^h(0)$ (solid lines), and center temperature rise at the substrate-deposit interface $\theta_D^0(0)$ (dashed lines), on the normalized center height h_0/w_0. The deposit is a paraboloid spot ($m=1$ in Eq. (6.1)) with fixed radius $R/w_0=2$. The heat conductivity ratios employed are $K^*\equiv K_D/K_S=10,1,0.1$.

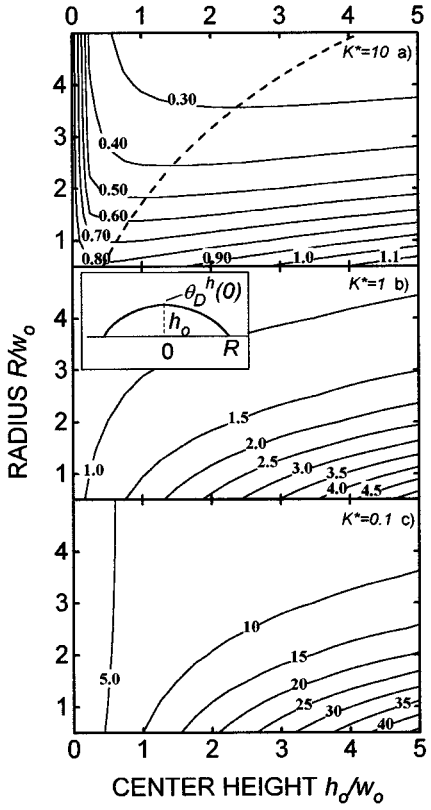

FIG. 5. The center temperature rise at the surface of the deposit $\theta_D^h(0)K_S/I_0Aw_0$ as the function of the height h_0/w_0 and radius R/w_0 for the paraboloid *spots* for different K^*. The geometry of the spot and the meaning of R, h_0 are illustrated in the inset. Surface absorption within the deposit. Dashed line shows the position of the *minimum* in $\theta_D^h(0)[h_0]$ dependence (see Fig. 3 for $K^*=10$) for different values of R.

It is illustrative to follow the behavior of the central temperature rise $\theta_D^h(0)$ with increasing height h_0 when the radius R is kept constant. The normalized dependences of $\theta_D^h(0)$, and center temperature at the substrate-deposit interface $\theta_D^0(0)$ on h, are presented in Fig. 4 for $R/w_0=2$ and different values of K^*. In all cases (normalized) $\theta_D^h(0)$ and $\theta_D^0(0)$ start from the value $0.5\pi^{1/2}\approx 0.88$ which corresponds to the plane semi-infinite substrate (see e.g., Eq. (5.1a) with $h=0$). With increasing h_0, there is a homogenization of the temperature within the plane $z=0$. As a result, θ_D^0 approaches limiting value. The limiting value for θ_S^0 (which is equal to θ_D^0 in this section) can be derived from the energy balance, corresponding to the uniform temperature[5] within the deposit $r<R$ at $z=0$.

$$P=\pi w_0^2 A I_0=4K_S\theta_S^0 R\Rightarrow\frac{\theta_D^0 K_S}{I_0 A w_0}=\frac{\pi w_0}{4R}. \tag{6.2}$$

Here P is the total absorbed power. The value of $\theta_D^h(0)$ for $K^*=1$ is much higher than $\theta_D^0(0)$, due to the temperature gradients within the deposit, which deliver the absorbed energy from $z=h$ to $z=0$. With high values of h_0, $\theta_D^h(0)$ increases linearly with h_0.

For moderate values of h_0 with $R/w_0>1$ and $K^*>1$, $\theta_D^h(0)$ establishes as a result of two competing factors: *lateral* spreading of the heat flux through the good conducting deposit which tends to decrease $\theta_D^h(0)$, and the increasing temperature difference between the surface of the deposit and deposit-surface interface which tends to increase $\theta_D^h(0)$. At small values of h_0, the first factor prevails, while later the second factor is more important, and $\theta_D^h(0)$ increases. Correspondingly, there exists a value of h_0/w_0 where $\theta_D^h(0)$ reaches its minimum. This value depends on K^*, as well as on R/w_0 which can be seen from the Fig. 5a, dashed line.

In Fig. 5 we present the results of calculations of the normalized center temperature rise at the surface of the deposit $\theta_D^h(0)K_S/I_0Aw_0$ as the function of both the height h_0/w_0 and radius R/w_0. We considered paraboloid *spots* (Eq. (6.1) with $m=1$), and three values of K^*. With $K^*<1$, $\theta_D^h(0)$ is always higher than the value 0.88 for the semiinfinite substrate. $\theta_D^h(0)$ increases with h_0 and decreases with R, because of the changes in the solid angle into which the heat can dissipate. With $K^*>1$, $\theta_D^h(0)$ *always* has a minimum as a function of h_0. The dashed line shows the position of this minimum for different values of R.

The example of a *self-consistent* calculation, which takes into account the growth of the spot is presented in Fig. 6. Here, the profile of height changes with time due to the deposition (normal to the surface at each point) according to the Arrhenius kinetics:

$$W(T)=W_0\ \exp(-T_a/T). \tag{6.3}$$

Details of the numerical procedure will be presented elsewhere. Parameters, used in calculations are listed in figure caption. They are close to values, corresponding to the pyrolytic deposition of Si from SiH_4[1,30,31] or C from CH_4 and C_2H_2 on quartz.[1,31] Figure 6 demonstrates the transition to an explosive growth regime, i.e., the formation of a fiber. Initially, center temperature decreases, due to better lateral heat conduction within the deposit, and later increases, due to increase in height and build up of the temperature difference within the deposit in z-direction. The radius of the spot (not shown) saturates in the initial stage of growth at a value $R/w_0\approx 1.24$ for lower intensity $I^*=5$, and at $R/w_0\approx 1.3$ for $I^*=6$. Qualitatively, $T(0)$ starts to increase, when during the growth, the spot enters the region to the right side of the

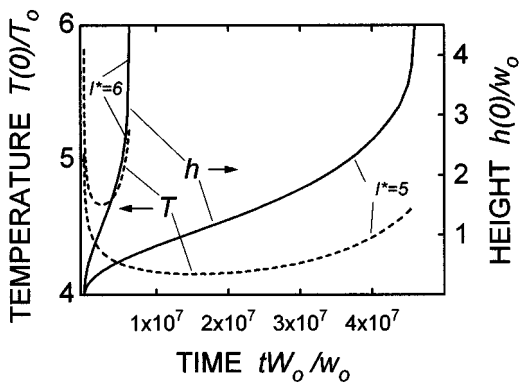

FIG. 6. The time-dependent behavior of the center height $h(0)$ (solid curve) and center temperature $T(0)$ (dashed curve) during the pyrolytic deposition of spots with kinetics of Eq. (6.3), for two different laser intensities (powers) $I^*=I_0Aw_0/K_ST_0=5,6$. The parameters employed are: $K_D/K_S=10$, $T_a/T_0=70$. With $T_0=300$ K, $w_0=10$ μm, $K_S=0.03$ W/cm K (fused SiO_2 at elevated temperatures, see Ref. 33), $W_0=10^4$ cm/s, $A=0.5$, this corresponds to $RT_a=41.8$ kcal/mol, laser power $P=283$ and 340 mW, and one unit of dimensionless time is equal to 10^{-7} s. These values are typical for the pyrolytic deposition of Si from SiH_4 on quartz substrates, see Refs. 1 and 31.

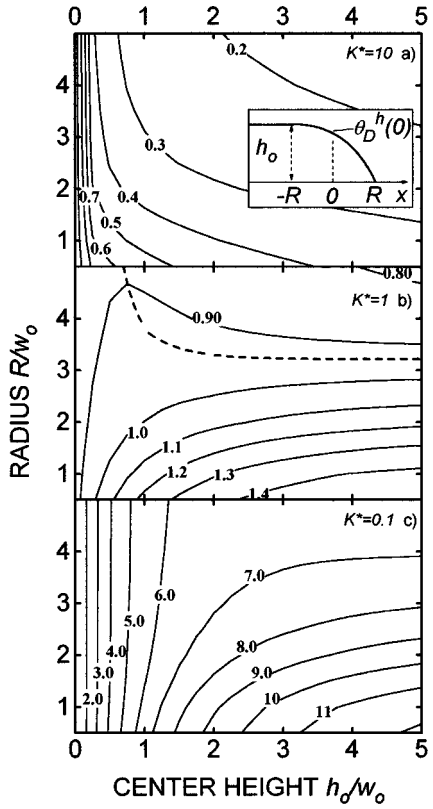

FIG. 7. The same as Fig. 5, but for the parabolic *stripes* ($m=1$ in Eq. (6.4)). The geometry of the stripe and the meaning of R, h_0 are shown in the inset. Dashed line shows the position of the *maximum* in $\theta_D^h(0)[h_0]$ dependence for different values of R.

dashed line in Fig. 5a. In other words, if the temperature starts to increase during the growth process, the growth rate increases as well. This leads to a further increase in height which further increases temperature. This feedback loop results in the formation of a growing fiber. For higher laser intensity I_0 (or power P) the time t_e to reach explosive growth regime is much shorter (note, that the difference in laser powers is only 20%). If the power is increased twofold, t_e decreases 5×10^2 times. This is due to the high activation energy employed. In case of scanning with velocity v_s, this time should be compared with the dwell time t_d of the beam. If $t_d(v_s)<t_e(P)$, the deposition proceeds in a direct writing regime. If $t_d(v_s)>t_e(P)$, the fiber grows towards the laser beam instead. Thus the condition of stripe to fiber transition[21,30] depends on both v_s and P.

Figure 7 is similar to Fig. 5, but for the parabolic ($m=1$) *stripes*, with the shape given by (see also inset in the Fig. 7):

$$h(\mathbf{r})=\begin{cases}\begin{cases}h_0(1-(y/R)^{2m}), & y<R\\ 0, & y>R,\end{cases} & x<-R\\ \max[0,\quad h_0(1-(y/R)^{2m}-((x-R)/2R)^{2m})], & x>-R.\end{cases} \tag{6.4}$$

Here x is the direction along the stripe. Expression (6.4) describes the profile of stripes, observed in the experiments on laser direct writing.[1] The height of the stripe reaches stationary value h_0 at a distance $x=-R$ *behind* the laser beam positioned at $\mathbf{r}=0$. For the *stripes* the position of maximum in temperature deviates slightly from the center of laser beam. However, this deviation is small, and we still considered $\theta_D^h(\mathbf{r}=0)$.

Figure 7a is similar to Fig. 5a, although for the particular values of parameters employed in calculations it *does not* exhibit an increase in $\theta_D^h(0)$ with h_0. Thus, the transition to the extensive growth (see Fig. 6) occurs at different parameters for the spots and the stripes. This may explain the *bistability* in this transition with respect to laser power and scanning velocity, observed experimentally.[1,21,30] Here the stripe-fiber transition occurred at different values of laser power, depending on whether power was gradually increased or decreased. With *increasing* laser power the fiber starts to grow from the continuous *stripe*. With *decreasing* power from the fiber-growth regime, the growth stops. Then, laser beam reaches the substrate and new fiber starts to grow from the initial stage of *spot*. This may happen at lower powers, than these required to grow the fiber from the *stripe*.

Figure 7b demonstrates new feature. For $K^*=1$, with R kept constant, (normalized) $\theta_D^h(0)$ first increases, and then decreases, and can reach the values *smaller* than 0.88 which

corresponds to a plain substrate. This can be understood, if we consider the front edge of the (big enough) stripe as the wedge, which permits the dissipation of heat into a solid angle *bigger* than 2π (half space). Another reason can be the oblique incidence of the laser beam, which increases the illuminated area. The dashed line shows the position of the maximum in $\theta_D^h(0)$ for different values of R. Such a decrease in $\theta_D^h(0)$, when aggravated by the strong dependence $T(\theta_D)$, may be responsible for the oscillations observed in the deposition of Si on Si (Ref. 1, p. 112). There, during the direct laser writing experiments, the deposit consisted of separated spots, despite continuous scanning. It can be due to the fact, that when certain height is reached, the temperature becomes so small, that further deposition is impossible.

Figure 7c is again similar to Fig. 5c with much smaller absolute values of θ_D^h due to much higher heat flux into the stripe, as compared to the spot.

VII. CONCLUSIONS

We present a procedure for fast calculation of the temperature distributions in the deposits of *arbitrary* shape on the semiinfinite substrates. Arbitrary temperature dependences in heat conductivities are allowed. The accuracy of the method was studied and was found to increase with increasing heat conductivity ratio K_D/K_S, or decreasing height of the deposit h. The procedure was used to find the central temperature in the deposited spots and stripes. The influence of the shape of the deposit on temperature distribution was investigated. This influence becomes more pronounced with decreasing heat conductivity of the deposit.

It is shown that for the *spots*, with $K_D/K_S>1$, there exists a height, which corresponds to a minimum central temperature. This is a result of competition between the lateral spreading of the heat within the deposit and the build up of the temperature differences between the surface of the deposit and the substrate-deposit interface.

For certain *stripes* with $K_D=K_S$ the maximum temperature can *decrease* as compared to the plane semiinfinite substrate.

The formalism can be applied to a simulation of the complex behavior observed in the experiments on laser direct writing of Si[1,30] and W[32] from gas phase precursors. We present an example of such *self-consistent* calculations which takes into account kinetics of deposition and demonstrates transition to the explosive growth (formation of a fiber).

The developed approach can also be useful in other areas where the solution of the Poisson equation for complex (probably time-dependent) geometries is required.

ACKNOWLEDGMENTS

The author wishes to thank Professor D. Bäuerle and Professor B. Luk'yanchuk for valuable discussions and the ''Fonds zur Förderung der Wissenschaftlichen Forschung in Österreich'' for financial support.

[1] D. Bäuerle, *Laser Chemical Processing* (Springer, Berlin, 1986); *Laser Processing and Chemistry* (Springer, Berlin, 1996).
[2] *Laser Microfabrication–Thin Film Processes and Lithography*, edited by D. J. Ehrlich and J. Y. Tsao (Academic, New York, 1989).
[3] *Laser and Particle-Beam Chemical Processing for Microelectronics*, edited by D. J. Ehrlich, G. S. Higashi, and M. M. Oprysko, Proc. MRS, Vol. 101 (North Holland, New York, 1987).
[4] T. H. Baum and P. B. Comita, Thin Solid Films **218**, 80 (1992).
[5] H. S. Carslaw and J. C. Jaeger, *Conduction of Heat in Solids* (Oxford University Press, New York, 1959).
[6] M. Lax, J. Appl. Phys. **50**, 3919 (1977).
[7] M. Lax, Appl. Phys. Lett. **33**, 786 (1978).
[8] M. L. Burgener and R. E. Reedy, J. Appl. Phys. **53**, 4357 (1982).
[9] E. Abraham and J. M. Halley, Appl. Phys. A **42**, 279 (1987).
[10] I. D. Calder and R. Sue, J. Appl. Phys. **53**, 7545 (1982).
[11] Y. I. Nissim, A. Lietoila, R. B. Gold, and J. F. Gibbons, J. Appl. Phys. **51**, 274 (1980).
[12] D. J. Ehrlich and J. Y. Tsao, J. Vac. Sci. Technol. B **1**, 969 (1983).
[13] D. J. Ehrlich, Appl. Surf. Sci. **69**, 115 (1993).
[14] K. Piglmayer, Ph.D. thesis, Linz, 1986.
[15] K. Piglmayer, J. Doppelbauer, and D. Bäuerle, in *Laser Controlled Chemical Processing of Surfaces*, edited by A. W. Johnson, D. J. Ehrlich, and H. R. Schlossberg (North Holland, New York, 1984), p. 47.
[16] T. T. Codas, T. H. Baum, and P. B. Comita, J. Appl. Phys. **61**, 2749 (1987).
[17] C. Garrido, B. Leon, and M. Perez-Amor, J. Appl. Phys. **69**, 1133 (1991).
[18] D. C. Skouby and K. F. Jensen, J. Appl. Phys. **63**, 198 (1987).
[19] J. Han and K. F. Jensen, J. Appl. Phys. **75**, 2240 (1994).
[20] N. Arnold and D. Bäuerle, Microelectron. Eng. **20**, 31 (1993).
[21] N. Arnold, P. B. Kargl, and D. Bäuerle, Appl. Surf. Sci. **86**, 457 (1994).
[22] N. Kirichenko, Y. Khavin, and N. Arnold (unpublished).
[23] N. Arnold and D. Bäuerle, Microelectron. Eng. **20**, 43 (1993).
[24] G. E. Korn and T. E. Korn, *Mathematical Handbook for Scientists and Engineers* (McGraw–Hill, New York, 1972).
[25] P. M. Morse and H. Feshbach, *Methods of Theoretical Physics* (McGraw–Hill, New York, 1953).
[26] P. S. Landa, *Oscillations of Distributed Systems* (Nauka, Moscow, 1984).
[27] J. Mathews and R. L. Walker, *Mathematical Methods of Physics* (W. A. Benjamin, New York, 1970).
[28] W. H. Press, S. A. Teukolsky, W. T. Vetterling, and B. P. Flannery, *Numerical Recipes in FORTRAN* (Cambridge University Press, New York, 1992), pp. 490, 531, 862.
[29] N. W. Ashcroft and N. D. Mermin, *Solid State Physics* (Holt, Rinehart & Winston, Philadelphia, 1976), p. 730.
[30] P. B. Kargl, R. Kullmer, and D. Bäuerle, Appl. Phys. A **57**, 577 (1993).
[31] J. Doppelbauer and D. Bäuerle, in *Interfaces Under Laser Irradiation*, edited by L. D. Laude, D. Bäuerle, and M. Wautelet, NATO ASI Series E, Vol. 134 (Martinus Nijhoff, Dordrecht, 1987), p. 277.
[32] P. B. Kargl, R. Kullmer, and D. Bäuerle, Appl. Phys. A **57**, 175 (1993).
[33] *American Institute of Physics Handbook*, edited by D. E. Gray (McGraw–Hill, New York, 1972).